Optical phase recovery in the dispersive Fourier transform

D. R. Solli,[a] S. Gupta, and B. Jalali
Department of Electrical Engineering, University of California, Los Angeles, California 90095, USA

(Received 7 August 2009; accepted 10 November 2009; published online 9 December 2009)

The dispersive Fourier transform permits real-time acquisition of optical spectra with analog-to-digital converters. The method utilizies the property that a signal's temporal envelope matches its spectral profile if sufficiently dispersed. Unfortunately, the dispersion demand can be substantial and signal losses in highly dispersive elements represent a significant challenge, especially outside the telecommunications band. We address this problem by experimentally demonstrating that a time-domain equivalent of the Gerchberg–Saxton algorithm removes the fundamental dispersion requirement in the dispersive Fourier transform. The algorithm recovers the phase from time-domain intensity measurements. © *2009 American Institute of Physics*. [doi:10.1063/1.3271678]

Many natural and artificial systems exhibit extremely rapid dynamics and transitory behavior that, although fleeting, have great importance for basic science and applications. Fast changes are often extremely difficult to probe, as conventional instruments generally lack the speed to capture them, particularly when the behavior is nonrepetitive. In high-throughput sensing, for example, it is often necessary to screen large sample volumes for the proverbial needle-in-the-haystack in a short time.

A technique capable of acquiring optical spectra in real time without repetitive measurement[1–6] has emerged. It has been applied to real-time absorption[1] and Raman[5] spectroscopy, the detection of optical rogue waves,[7] high-speed imaging,[8] and other contexts. Chirped wavelength encoding and electronic time-domain sampling (CWEETS) or the dispersive Fourier transform employs group-velocity dispersion (GVD) to chirp a pulsed signal so that its spectrum can be measured in time using a photodetector and an oscilloscope in lieu of a conventional spectrometer.

The primary practical limitation of the technique lies in the propagation loss in the dispersive element. At telecommunications wavelengths (~1550 nm), low-loss dispersive fiber is readily available, but single-mode fibers are much more dissipative at other wavelengths of interest such as the visible and near-IR bands, which are particularly important for the study of rapid phenomena in biological applications. Even at 1550 nm, losses become appreciable for long fibers. In chip-scale applications, it has also proven to be extremely challenging to produce low-loss dispersive elements. Furthermore, even without dissipation, the act of dispersing a signal reduces its peak power level. *In situ* Raman amplification can soften these limitations[5] but it is nevertheless desirable to reduce the dispersion requirement. Unfortunately, the spectral shape is not properly transferred to time if the dispersion becomes too small.

Insufficient dispersion produces a particular type of distortion in the measured waveform. In analogy with spatial optics, we refer to this regime as the temporal near-field or the incomplete dispersive Fourier transform, whereas, the undistorted mapping is achieved in the temporal far-field. In the near-field, the profile is distorted, particularly when the spectrum contains multiple close features. Nevertheless, we demonstrate here that two independent time-domain near-field measurements can be used to recover the optical phase, permitting spectral reconstruction. To retrieve the phase, we employ a time-domain analog of the Gerchberg–Saxton (GS) algorithm. The GS algorithm is normally employed to retrieve the phase of a spatial image based on intensity measurements on two distinct planes;[9,10] however, an adaptation of this concept is suitable for the present problem. Previously, the GS algorithm has been employed to improve the SNR in photonic time-stretch analog-to-digital conversion.[11]

Figure 1 shows simulated temporal near-field profiles from representative absorption lines. The distortion mani-

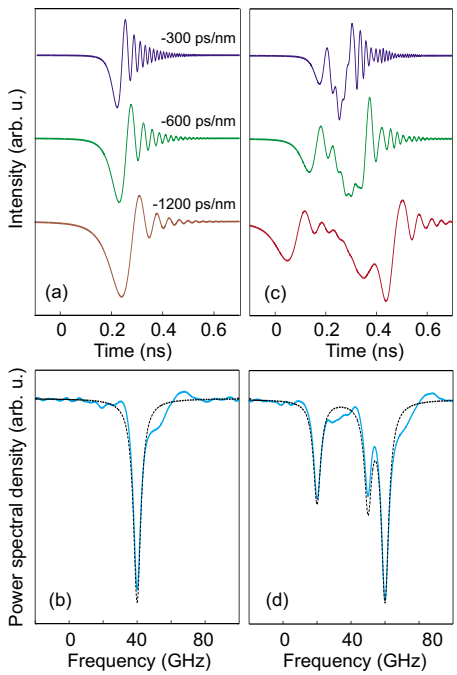

FIG. 1. (Color online) (a) Near-field waveforms from one absorption line (5 GHz width) after −300 ps/nm (blue), −600 ps/nm (green), and −1200 ps/nm (red). (b) Reconstruction of spectral line by temporal GS algorithm (cyan); actual spectrum (black, dashed). (c) Near-field waveforms from three close 5 GHz absorption lines after −300 ps/nm (blue), −600 ps/nm (green), and −1200 ps/nm (red). (d) Reconstructed spectrum of the three lines (cyan); actual spectrum (black, dashed). Frequency axis offset is arbitrary.

[a]Electronic mail: solli@ucla.edu.

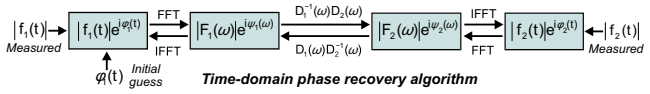

FIG. 2. (Color online) Schematic of the time-domain phase-recovery algorithm.

fests as rapid, chirped ringing on the trailing edge of the vestigial time-domain absorption line. With more dispersion, the line depth increases while the ripple frequency and amplitude decrease. For multiple lines in close proximity, the patterns from different lines interfere, leading to a convoluted near-field trace.

The distribution of the ripples can be traced to causality. If the absorption line is applied without a causal phase shift, the ripples appear on both edges of the temporal lineshape. The ripples arise due to interference between the wavelength components, which have not been fully separated in time and do not have the proper amplitudes and phases to sum to the original pulse profile. Thus, both amplitude and phase information are encoded onto the near-field envelope. The algorithm extracts this information (cf. Fig. 1).

Prior to describing the algorithm in detail, we consider the near-field spectral resolution. As for all measurements, the intrinsic spectral resolution originates from the measurement duration and is independent of any applied dispersion. A narrow feature can be probed by an ultrashort optical pulse because the repetition period, not the pulse duration, defines the spectral resolution per the uncertainty principle. Likewise, the spectral resolution of CWEETS is ultimately limited by the pulse repetition frequency of the source (comb line spacing), just as in any measurement.

Yet, an undistorted profile cannot be achieved with inadequate dispersion as the lineshape must be sufficiently stretched to satisfy the uncertainty principle. This concept can be noted in Fig. 1, where the duration of the lineshape plus distortion remains approximately constant regardless of the dispersion. With further dispersion, the line eventually becomes wide enough to satisfy the uncertainty principle without distortion. At this point, its envelope bandwidth $\Delta\nu$ must be less than or equal to its optical bandwidth. The uncertainty principle specifies $\Delta\nu\Delta\tau \sim 1/2$, where $\Delta\tau$ is the temporal duration of the lineshape and is determined by the GVD parameter D, the length of the fiber z, and the wavelength width $\Delta\lambda$ of the spectral line: $\Delta\tau \sim |D|z\Delta\lambda$. These expressions yield the uncertainty-principle-limited dispersion for an undistorted lineshape: $|D|z \sim [1/(2c)](\lambda/\Delta\lambda)^2 \sim [1/(2c)](\nu/\Delta\nu)^2$, where c is the speed of light and λ and ν are the line's center wavelength and frequency.

Narrow spectral features may require a prohibitively large amount of dispersion to be fully mapped into time, but the oscilloscope may have sufficient electronic bandwidth to capture the near-field waveform. We also note that for a feature of linewidth $\Delta\nu$, it requires more dispersion to produce an undistorted lineshape at shorter wavelengths; thus, the need for reconstruction becomes paramount at visible wavelengths because of increases in both the loss per unit fiber length and the dispersion requirement itself.

The algorithm is illustrated schematically in Fig. 2. The procedure for reconstruction requires that the temporal envelope of the signal be recorded with two different values of dispersion D_1 and D_2, producing the time-domain measurements $|f_1(t)|$ and $|f_2(t)|$, respectively. To begin the procedure, an initial guess for the phase is required; since $f_1(t)$ has been chirped by D_1, a reasonable choice can be obtained from a chirped pulse of the proper bandwidth. The phase guess and measured magnitude are combined and numerically Fourier transformed to the frequency domain, the quadratic phase due to dispersion $f_1(t)$ is then removed and D_2 is applied, and the waveform is transformed back to time. At this point, the magnitude is replaced by the measurement $|f_2(t)|$ and the phase is retained. The procedure is then run in reverse, utilizing the measurement $|f_1(t)|$ again at the opposite end. This process is repeated at the user's discretion; as shown in Fig. 3, the errors in the magnitude (determined prior to application of $|f_1(t)|$ and phase decrease with additional iterations. Once the phase has been recovered, the waveform's Fourier transform can be computed. Higher-order dispersion, which may be needed for wide spectral windows, can be readily included and is implemented in our experimental reconstruction described below.

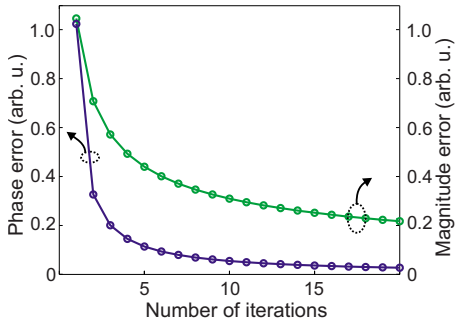

FIG. 3. (Color online) Phase (left axis) and magnitude (right axis) errors vs iterations of the temporal algorithm ($D_1 = -600$ ps/nm, $D_2 = -900$ ps/nm). The errors are defined as: $\varepsilon_{\text{phase},n} = \sqrt{\Sigma|\varphi_{1,n}(t) - \varphi_{1,n-1}(t)|^2}$ and $\varepsilon_{\text{magnitude},n} = \sqrt{\Sigma||f_{1,n}(t)|^2 - |f_1(t)|^2|^2}$, where $|f_{1,n}(t)|^2$ is the intensity envelope after n iterations, $|f_1(t)|^2$ is the measured envelope with D_1, and $\varphi_{1,n}(t)$ is the phase of $f_{1,n}(t)$. The iteration number is defined as the number of envelope replacements. Errors are calculated just prior to the $f_1(t)$ replacement.

For efficient convergence, the two measurements should have sufficient diversity. Otherwise, there is no basis for iteration, and the algorithm returns the initial phase guess. Some spectral recovery can be obtained by the phase guess alone, but ripple artifacts appear on one side of the spectral feature. With greater diversity, the spectral error is reduced and small ripples, which diminish with additional iterations, appear on both sides of the line (cf. Fig. 4).

We also test the algorithm experimentally using the apparatus illustrated in Fig. 5(a). Near-transform-limited

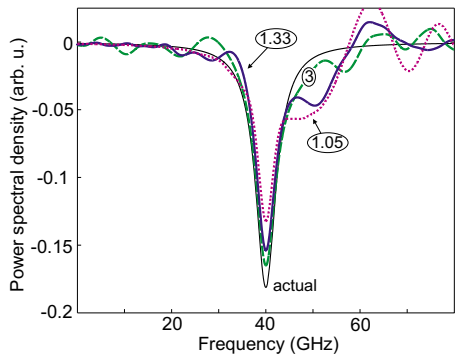

FIG. 4. (Color online) Recovered spectrum of a 5 GHz line after 20 iterations with $D_1 = -600$ ps/nm and $D_2/D_1 = 1.05$ (purple), $D_2/D_1 = 1.33$ (blue), and $D_2/D_1 = 3$ (green). Arbitrary frequency axis offset.

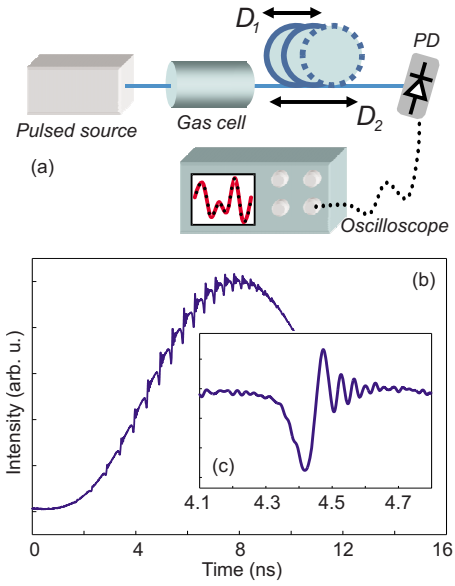

FIG. 5. (Color online) (a) Experimental setup for near-field measurements: $D_1 \sim -695$ ps/nm, $D_2 \sim -800$ ps/nm. (b) Pulse with encoded absorption lines measured with near-field dispersion D_1. (c) Closeup view of a near-field absorption line.

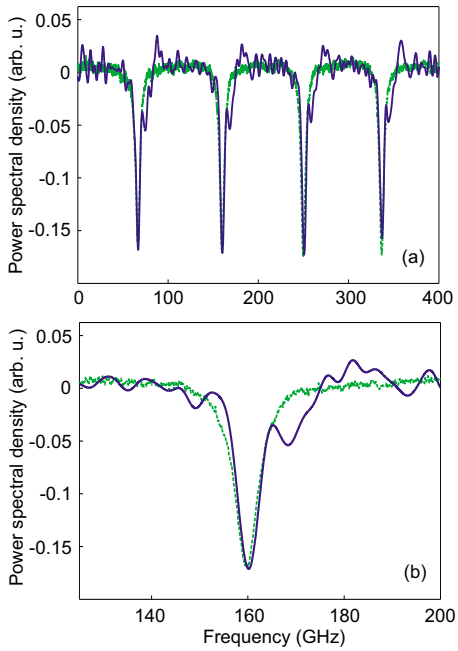

FIG. 6. (Color online) (a) Reconstructed gas spectrum from near-field measurements with $D_1 \sim -695$ ps/nm, $D_2 \sim -800$ ps/nm and 20 iterations with the temporal GS algorithm (blue trace). Spectrum recorded with optical spectrum analyzer also shown (green trace, dashed). (b) Closeup view of a reconstructed line. Arbitrary frequency axis offset.

pulses from a mode-locked laser ($\lambda_0 = 1563$ nm, $\Delta\lambda \sim 10$ nm, 36 MHz rep. rate) travel through a carbon monoxide gas cell. The transmitted light is directed separately through the dispersive elements $D_1 \sim -695$ ps/nm and $D_2 \sim -800$ ps/nm and the signals are recorded with a photodiode and sampling oscilloscope (electrical bandwidth ~40 GHz). As seen in Figs. 5(b) and 5(c), the near-field patterns of multiple absorption lines are encoded onto the pulse.

Figure 6 shows the spectrum recovered from the experimental data. The algorithm simultaneously operates on all the absorption lines, producing a spectrum that compares well with that obtained from a spectrometer. The fiber's dispersion slope was included in the reconstruction. We note that the recovered spectrum has peaklike artifacts on the trailing edges of the absorption lines, similar to the small ghost peaks seen in simulations when the ratio of dispersive elements is close to unity (cf. Fig. 4). These features are relatively minor and do not affect the recovered full width at half maximum linewidth. In addition, their locations are systematic, making them straightforward to recognize. We have also observed that the spectral error is minimized with a moderate number of iterations. This effect may arise from accumulated measurement distortions (e.g., optical nonlinearities and electronic bandwidth limitations); but, as the departure occurs slowly, the appropriate number of iterations can be predetermined. For proper reconstruction, the oscilloscope must have sufficient time resolution (bandwidth): a minimum estimate can be obtained from the target spectral resolution and the smaller dispersion value. The electronic bandwidth is sufficient if increases in dispersion do not substantially affect reconstruction.

A sampling scope was utilized in this proof-of-principle demonstration for its wide bandwidth. For real-time measurements, commercial real-time analog-to-digital converters (ADCs) can offer sufficient bandwidth for near-field capture depending on the linewidth and dispersion. Moreover, ADC speeds are being continually improved in the quest for faster communications. Going beyond the bandwidths of purely electronic ADCs, near-field capture can also be performed with optically enhanced ADCs.[12,13] One useful method, the photonic time-stretch ADC, requires dispersive elements itself; however, it operates at 1550 nm and, therefore, shifts the dispersive burden away from problematic wavelengths.

In conclusion, we have demonstrated that a GS-inspired algorithm can be used to extend the capabilities of CWEETS spectroscopy, eliminating the fundamental dispersion requirement in the dispersive Fourier transform. Finally, we point out that a temporal GS algorithm may also have application in other contexts. For example, the so-called time-lens method—the temporal analog of spatial imaging—normally relies on a specific condition to produce a focused temporal image.[14] However, the temporal image may be recovered from two unfocused signals, just as reconstruction is accomplished in spatial imaging.

This work was supported by DARPA and NSF.

[1]P. V. Kelkar, F. Coppinger, A. S. Bhushan, and B. Jalali, Electron. Lett. **35**, 1661 (1999).
[2]Y. C. Tong, L. Y. Chan, and H. K. Tsang, Electron. Lett. **33**, 983 (1999).
[3]S. T. Sanders, Appl. Phys. B: Lasers Opt. **75**, 799 (2002).
[4]J. Hult, R. S. Watt, and C. F. Kaminski, Opt. Express **15**, 11385 (2007).
[5]D. R. Solli, J. Chou, and B. Jalali, Nat. Photonics **2**, 48 (2008).
[6]H. R. Fetterman, P. E. Tannenwald, C. D. Parker, J. Melngailis, and R. C. Williamson, Appl. Phys. Lett. **34**, 123 (1979).
[7]D. R. Solli, C. Ropers, and B. Jalali, Nature (London) **450**, 1054 (2007).
[8]K. Goda, K. K. Tsia, and B. Jalali, Nature (London) **458**, 1145 (2009).
[9]R. W. Gerchberg and W. O. Saxton, Optik (Stuttgart) **35**, 237 (1972).
[10]J. R. Fienup, Appl. Opt. **21**, 2758 (1982).
[11]J. Stigwall and S. Galt, *Proceedings of the International Topical Meeting on Microwave Photonics*, Grenoble (IEEE, Piscataway, NJ, 2006), p. 1.
[12]Y. Han and B. Jalali, J. Lightwave Technol. **21**, 3085 (2003).
[13]G. C. Valley, Opt. Express **15**, 1955 (2007).
[14]B. H. Kolner, IEEE J. Quantum Electron. **30**, 1951 (1994).